6-1-2007

Characterization of the Catalytically Active Mn(II)-loaded *argE*-encoded *N*-acetyl-L-ornithine Deacetylase from *Escherichia coli*

Wade C. McGregor
Utah State University

Sabina I. Swierczek
Utah State University

Brian Bennett
Marquette University, brian.bennett@marquette.edu

Richard C. Holz
Marquette University, richard.holz@marquette.edu

Accepted version. *Journal of Biological Inorganic Chemistry*, Vol. 12, No. 5 (June 2007): 603-613.

Brian Bennett was affiliated with the Medical College of Wisconsin at the time of publication.
Richard Holz was affiliated with Loyola University-Chicago and Utah State University at the time of publication.

Journal of Biological Inorganic Chemistry, Vol. 12, No. 5 (June 2007): 603-613. DOI.

Characterization of the catalytically active Mn(II)-loaded *argE*-encoded *N*-acetyl-l-ornithine deacetylase from *Escherichia coli*

Wade C. McGregor
The Department of Chemistry and Biochemistry Utah State University Logan USA

Sabina I. Swierczek
The Department of Chemistry and Biochemistry Utah State University Logan USA

Brian Bennett
The Department of Physics, Marquette University, Milwaukee, WI USA
The National Biomedical EPR Center, Department of BiophysicsMedical College of WisconsinMilwaukeeUSA

Richard C. Holz
The Department of Chemistry, Marquette University, Milwaukee, WI USA
The Department of Chemistry Loyola University Chicago Chicago USA
The Department of Chemistry and Biochemistry Utah State University Logan USA

Abstract

The catalytically competent Mn(II)-loaded form of the *argE*-encoded *N*-acetyl-l-ornithine deacetylase from *Escherichia coli* (ArgE) was characterized by kinetic, thermodynamic, and spectroscopic methods. Maximum *N*-

acetyl-l-ornithine (NAO) hydrolytic activity was observed in the presence of one Mn(II) ion with k_{cat} and K_m values of 550 s^{-1} and 0.8 mM, respectively, providing a catalytic efficiency (k_{cat}/K_m) of 6.9×10^5 M^{-1} s^{-1}. The ArgE dissociation constant (K_d) for Mn(II) was determined to be 0.18 μM, correlating well with a value obtained by isothermal titration calorimetry of 0.30 μM for the first metal binding event and 5.3 μM for the second. An Arrhenius plot of the NAO hydrolysis for Mn(II)-loaded ArgE was linear from 15 to 55 °C, suggesting the rate-limiting step does not change as a function of temperature over this range. The activation energy, determined from the slope of this plot, was 50.3 kJ mol^{-1}. Other thermodynamic parameters were $\Delta G^{\ddagger}$ = 58.1 kJ mol^{-1}, $\Delta H^{\ddagger}$ = 47.7 kJ mol^{-1}, and $\Delta S^{\ddagger}$ = –34.5 J mol^{-1} K^{-1}. Similarly, plots of lnK_m versus 1/T were linear, suggesting substrate binding is controlled by a single step. The natural product, [(2*S*,3*R*)-3-amino-2-hydroxy-4-phenylbutanoyl]leucine (bestatin), was found to be a competitive inhibitor of ArgE with a K_i value of 67 μM. Electron paramagnetic resonance (EPR) data recorded for both [Mn(II)_(ArgE)] and [Mn(II)Mn(II)(ArgE)] indicate that the two Mn(II) ions form a dinuclear site. Moreover, the EPR spectrum of [Mn(II)Mn(II)(ArgE)] in the presence of bestatin indicates that bestatin binds to ArgE but does not form a μ-alkoxide bridge between the two metal ions.

Keywords

Hydrolysis, Manganese, Electron paramagnetic resonance, Antibiotics, Electronic absorption

Abbreviations

AAP	Leucine aminopeptidase from *Aeromonas proteolytica* (*Vibrio proteolyticus*)
ArgE	*argE*-encoded *N*-acetyl-l-ornithine deacetylase
Bestatin	[(2*S*,3*R*)-3-Amino-2-hydroxy-4-phenylbutanoyl]leucine
blLAP	Bovine lens leucine aminopeptidase
CPG_2	Carboxypeptidase G_2 from *Pseudomonas* sp. strain RS-16
DapE	*N*-Succinyl-l,l-diaminopimelic acid desuccinylase
EPR	Electron paramagnetic resonance
HEPES	4-(2-Hydroxyethyl)-1-piperazineethanesulfonic acid
ITC	Isothermal titration calorimetry
NAO	*N*-Acetyl-l-ornithine

Introduction

The emergence of antibiotic-resistant bacterial infections has created a significant and growing medical problem in the USA and throughout the world [1, 2, 3, 4]. Antibiotic resistance has been recognized since the introduction of penicillin more than 50 years ago when penicillin-resistant infections caused by *Staphylococcus aureus* rapidly appeared [3, 5]. Because bacteria have been exposed to many of the currently available antibiotics, such as *β*-lactams, fluoroquinolones, macrolides, tetracyclines, aminoglycosides, glycopeptides, or trimethoprim combinations, for years, they have evolved resistance to these drugs [3, 6, 7, 8, 9]. In fact, several bacterial infections, some of which were thought to have been eradicated, have made a significant resurgence owing to bacterial resistance to antibiotics. These illnesses include, but are not limited to, tuberculosis, staph infections, and childhood bacterial meningitis or ear infections [3, 5]. In addition to its adverse effect on public health, antimicrobial resistance contributes to higher health care costs. Treating resistant infections often requires the use of more expensive or more toxic drugs, such as colistin, and can result in longer hospital stays for infected patients [10]. The Institute of Medicine, a part of the National Academy of Sciences, has estimated that the annual cost of treating antibiotic-resistant infections in the USA may be as high as $30 billion [1]. Since many of the broad-spectrum antibiotics contain *β*-lactam functional units that target enzymes involved in bacterial cell wall synthesis or pathways involved in cell replication [3, 5], new enzymatic targets must be located so novel inhibitors can be synthesized, providing new classes of antibiotics. For this reason, several bacterial metallohydrolases containing dinuclear active sites have become the subject of intense efforts in inhibitor design [11, 12, 13, 14, 15, 16].

The *argE*-encoded *N*-acetyl-l-ornithine deacetylase (ArgE) is a bacterial metallohydrolase that contains a dinuclear active site and is a member of the arginine biosynthetic pathway in bacteria [17]. Prokaryotes synthesize arginine through a series of eight enzyme-catalyzed reactions that differ from those of eukaryotes in two key steps: (1) acetylation of glutamate and (2) the subsequent deacetylation of the arginine precursor *N*-acetyl-l-ornithine (NAO) by ArgE [18]. Because ornithine is required, not only for the synthesis of arginine in bacteria, but also for polyamines involved in DNA replication and cell division, NAO deacetylation is critical for bacterial proliferation [19]. Indeed, when Meinnel et al. [20] transformed an arginine auxotrophic bacterial strain void of NAO deacetylase activity with a plasmid containing *argE*, an Arg^+ phenotype resulted [20]. However, when the start codon (ATG) of *argE* in the same plasmid was changed to the Amber codon (TAG), the resultant plasmid was unable to relieve arginine auxotrophy in the same cell strain; therefore, ArgE is required for cell viability. Given the fact that ArgE is only found in prokaryotes and is required for bacterial cell growth and proliferation, it represents an enzymatic target for a novel class of antibacterial pharmaceuticals [19].

Though little is currently known about ArgE, it shares high sequence homology with several dinuclear metallopeptidases in family M28, some of which have been characterized in detail using kinetic, spectroscopic, and crystallographic methods [21]. High-resolution X-ray crystal structures of the leucine aminopeptidase from *Aeromonas proteolytica* (*Vibrio proteolyticus*) (AAP) [22] and the carboxypeptidase G_2 from *Pseudomonas* sp. strain RS-16 (CPG_2) [23] revealed that these enzymes contain nearly identical active sites. To date, no X-ray crystallographic data have been reported for ArgE; however, all of the amino acids that function as metal ligands in AAP and CPG_2 are fully conserved in ArgE [21]. AAP and other M28 family members are competitively inhibited by synthetic small molecules classified as boronic acids [24, 25, 26], chloromethyl ketones [27], phosphonic acids [28, 29, 30], hydroxamates [31, 32, 33], and *β*-hydroxyamides [27]. The number of compounds isolated from natural sources capable of inhibiting aminopeptidases is also increasing. For instance, [(2*S*,3*R*)-3-amino-2-hydroxy-4-phenylbutanoyl]leucine (bestatin), a dipeptide isolated from cultures of *Streptomyces olivoreticuli* [34], exhibits slow-binding inhibition towards bovine lens leucine aminopeptidase (blLAP) and AAP with K_i^* values of 1.3 and 18 nM, respectively [35]. These small molecule inhibitors are effective owing to complexation of the active-site metal ions and this complexation is a function of both the particular metal ion involved and the catalytic mechanism of the enzyme. In order to determine if ArgE can be activated by Mn(II) ions, similar to blLAP [36], we have examined the Mn(II)-loaded ArgE enzyme from *Escherichia coli* using both kinetic and spectroscopic methods. These data indicate that ArgE can be activated by Mn(II) ions and confirm that dinuclear Mn(II) centers are formed. These data also provide additional information regarding the enzymatic mechanism of ArgE, an important precursor to the rational design of a new class of ArgE inhibitors that potentially exhibit therapeutic functions.

Materials and methods

Enzyme expression and purification

All chemicals used in this study were purchased from commercial sources and were of the highest quality available. ArgE from *E. coli* was purified as previously described [17] from a stock culture provided by John Blanchard [21]. The purified enzyme exhibited a single band on a 12% sodium dodecyl sulfate polyacrylamide gel electrophoresis gel, which corresponds to its calculated M_r of 42,350, by comparison with molecular weight standards purchased from Sigma. It was subsequently concentrated to below 1 mM and stored at 4 °C. Protein concentrations were determined using the theoretical value ε_{280} = 41,250 M^{-1} cm^{-1} [37].

Preparation of apo enzymes

Divalent metal ions were removed from ArgE by dialysis against more than 500 vol of 10 mM EDTA in 25 mM 4-(2-hydroxyethyl)-1-piperazineethanesulfonic acid (HEPES), pH 7.5, for at least 48 h at 4 °C. EDTA was removed by extensive dialysis against 50 mM Chelex-100 treated HEPES buffer, pH 7.5, at 4 °C. Metals were removed from all dialysisware by incubation in 10 mM EDTA, pH 8.0, for more than 48 h. HEPES was made “metal-free” by

passing it through a Chelex-100 column. ArgE thus treated was inactive and found to contain no detectable metals ions via inductively coupled plasma atomic emission spectrometry.

Enzymatic assay of ArgE

Unless otherwise noted, enzyme kinetic constants were determined in 50 mM Chelex-100 treated sodium phosphate buffer, pH 7.5, with NAO as the substrate at 25 °C. The rate of NAO deacetylation was monitored as a decrease in absorbance at 214 nm. Catalytic activities were determined within ±10%. Initial rates were fit directly to the Michaelis–Menten equation to obtain the catalytic constants K_m and k_{cat}. The monosubstituted species [Mn(II)_(ArgE)] was prepared by incubating apo-ArgE with one stoichiometric equivalent of metal, while the disubstituted species [Mn(II)Mn(II)(ArgE)] was generated by incubating apo enzyme with 2 equiv of Mn(II) for approximately 20 min at 25 °C.

Isothermal titration calorimetry

Isothermal titration calorimetry (ITC) measurements were carried out on a MicroCal OMEGA ultrasensitive titration calorimeter. The divalent metal ion titrant and apo enzyme solutions were prepared in Chelex-100 treated 25 mM HEPES buffer, pH 7.5. Stock buffer solutions were thoroughly degassed before each titration. The enzyme solution (70 µM) was placed in the calorimeter cell and stirred at 200 rpm to ensure rapid mixing. Typically, 4–6 µL of titrant was delivered over 7.6 s with a 6-min interval between injections to allow for complete equilibration. Each titration was continued until 4.5–6 equiv of Mn(II) had been added to ensure that no additional complexes were formed in excess titrant. A background titration, consisting of the identical titrant solution but only the buffer solution in the sample cell, was subtracted from each experimental titration to account for the heat of dilution. These data were analyzed with a two-site binding model by the Windows-based Origin software package supplied by MicroCal. The equilibrium binding constant, K_a, and the enthalpy change, ΔH, were used to calculate ΔG and ΔS using the Gibbs free energy relationship (Eq. 1):

$$\Delta G^\circ = -RTK_a = \Delta H^\circ - T\Delta S^\circ \qquad (1)$$

where R = 1.9872 cal mol^{-1} K^{-1}. The relationship between K_a and K_d is defined as

$$K_d = 1/K_a \qquad (2)$$

Individual ArgE solutions were prepared by diluting stock enzyme solutions in 25 mM Chelex-100 treated HEPES buffer, pH 7.6, containing 150 mM KCl.

Spectroscopic measurements

Kinetic data were recorded using a Shimadzu UV-3101PC spectrophotometer. The temperature of assay solutions and that of the cuvette cavity were maintained by a circulating water bath (Isotemp 20130D, Fischer Scientific). Low-temperature electron paramagnetic resonance (EPR) spectroscopy was performed using a Bruker Elexsys E500 spectrometer equipped with an ER 4116 DM dual-mode X-band cavity and an Oxford Instruments ESR-900 helium-flow cryostat. Background spectra recorded on a buffer sample were aligned with and subtracted from experimental spectra as described previously [38, 39]. EPR spectra were recorded with 20-mW microwave power (in a Bruker ER4116DM cavity in $\boldsymbol{B}_{microwave} \perp \boldsymbol{B}_{static}$ mode) at 9.6330 ± 0.0005 GHz, 6–30 K, and with 10.6 G magnetic field modulation at 100 kHz. The species termed here "[Mn(II)_(ArgE)]" and "[Mn(II)Mn(II)(ArgE)]" correspond to apo-ArgE to which 1 and 2 equiv of Mn(II) were added, respectively; [Mn(II)Zn(II)(ArgE)] denotes ArgE to which first 1 equiv of Mn(II) was added, followed by 1 equiv of Zn(II), and [Zn(II)Mn(II)(ArgE)] refers to ArgE to which first 1 equiv of Zn(II) was added, followed by 1 equiv of Mn(II).

Results

Catalytic activity of Mn(II)-loaded ArgE

Incubation of apo-ArgE with 1 equiv of Mn(II) produced an enzyme with a k_{cat} value of 550 s^{-1}, which is 2.8-fold lower than that observed for [Zn(II)_(ArgE)] and 4.6-fold lower than for [Co(II)_(ArgE)] [17] (Table 1). The observed K_m value for NAO binding to [Mn(II)_ArgE] is identical (0.8 mM) within error to that observed for Zn(II)-loaded ArgE. The k_{cat} value for NAO hydrolysis by ArgE as a function of Mn(II) concentration was also examined. In these studies, 100 µM ArgE was incubated with a preincubated number of metal equivalents for 20 min at 25 °C before kinetic analyses were performed (Fig. 1). Maximum activity was observed at approximately 1 equiv of added Mn(II), with a slight decrease in k_{cat} upon further addition of up to 2 equiv of (Mn(II), similar to Zn(II) binding to ArgE [17]. The dissociation constant (K_d) for Mn(II) binding to ArgE was determined by fitting the activity titration data to Eq. 3 (Fig. 2) [17]:

$$r = pC_S/(K_d + C_S) \qquad (3)$$

where p is the number of sites for which interaction with Mn(II) is governed by the intrinsic dissociation constant, K_d, and r is the binding function calculated by the conversion of the fractional saturation (f_a) using Eq. 4:

$$r = f_a p \qquad (4)$$

C_S, the free metal concentration, was calculated using Eq. 5:

$$C_S = C_{TS} - rC_A, \qquad (5)$$

where C_{TS} and C_A are the total molar concentrations of metal and enzyme, respectively. A value for K_d was obtained by fitting the data via an iterative process that allowed both K_d and p to vary. The best fits obtained provided a p value of 1 and a K_d value of 0.18 µM.

Table 1. Kinetic constants for the hydrolysis of NAO catalyzed by [Mn(II)_(ArgE)] compared with those for NAO catalyzed by [Zn(II)_(ArgE)] and [Co(II)_(ArgE)] [17]

Enzyme form	k_{cat} (s^{-1})	K_m (mM)	k_{cat}/K_m (M^{-1} s^{-1})
[Zn(II)_(ArgE)]	1,600	0.8	2.0×10^6
[Co(II)_(ArgE)]	3,800	1.2	3.2×10^6
[Mn(II)_(ArgE)]	550	0.8	6.9×10^5

NAON-acetyl-l-ornithine, *ArgEargE*-encoded *N*-acetyl-l-ornithine deacetylase

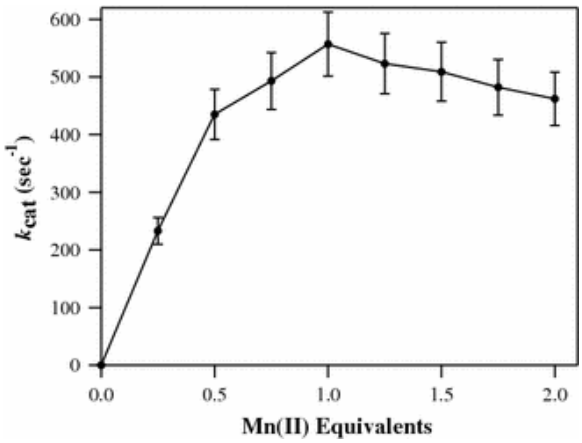

Fig. 1. k_{cat} of a 10 µM sample of apo *argE*-encoded *N*-acetyl-l-ornithine deacetylase (ArgE) titrated with 0.2–2.0 equiv of Mn(II)

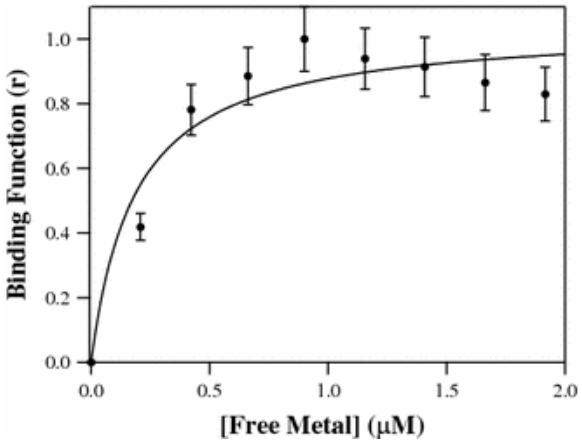

Fig. 2. Binding function (*r*) versus the concentration of free metal ions in solution (C_S) for Mn(II) titration into apo-ArgE (50 mM $KHPO_4$ buffer pH 7.5)

Isothermal titration calorimetry

ITC measurements were carried out using a MicroCal OMEGA ultrasensitive titration calorimeter at 25 ± 0.2 °C. Association constants (K_a) were obtained by fitting these data, after subtraction of the background heat of dilution, via an interactive process using the Origin software package (Fig. 3). The K_a value, enzyme-metal stoichiometry (*n*), and the change in enthalpy ($\Delta H°$) were allowed to vary during the fitting process. For ArgE, K_d values determined for Mn(II) binding revealed one tight binding site with a K_d value of 0.3 µM, while the second metal binding site exhibited weaker Mn(II) affinity, with a K_d value of 5.3 µM. The thermodynamic properties observed for Mn(II) binding were similar to those monitored for Zn(II) binding to ArgE for the first metal binding event, which is endothermic. However, the second binding event is also endothermic for Mn(II), but exothermic for Zn(II) (Table 2).

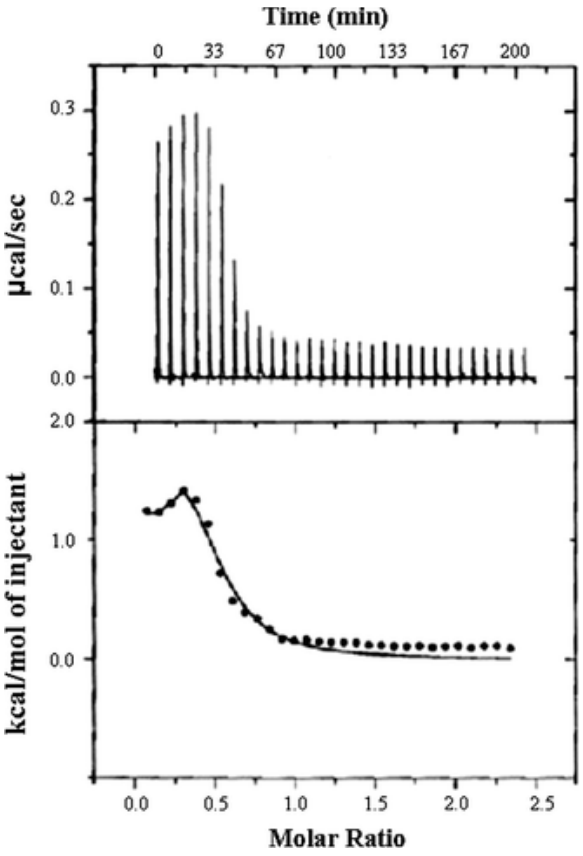

Fig. 3. a Isothermal titration calorimetry (ITC) titration of a 70 µM solution of apo-ArgE with a 2.5 mM solution of Mn(II). **b** Fit of the ITC data for ArgE after subtraction of the heat of dilution. Reaction conditions, 25 °C in 50 mM 4-(2-hydroxyethyl)-1-piperazineethanesulfonic acid (HEPES) buffer, pH 7.5, and 150 mM KCl

Table 2. Thermodynamic parameters for binding of ArgE to Mn(II) compared with those previously determined for binding of ArgE to Zn(II) and Co(II) [17]

Parameter	Zn(II)	Co(II)	Mn(II)
ΔH_1 (kcal mol^{-1})	4.6	2.2	1.2
ΔH_2 (kcal mol^{-1})	−2.7	−26.0	2.0
ΔG_1 (kcal mol^{-1})	−5.9	−8.7	−8.8
ΔG_2 (kcal mol^{-1})	−7.6	−5.2	−7.2
ΔS_1 (cal mol^{-1} K^{-1})	35	36	33
ΔS_2 (cal mol^{-1} K^{-1})	16	−70	30

Temperature dependence of NAO hydrolysis by Mn(II)-loaded ArgE

The hydrolysis of NAO by ArgE, loaded with 1 or 2 equiv of manganese, was linear over the temperature range 15–55 °C. Because $V_{max}/[E] = k_p$ (where [E] is the enzyme concentration), in rapid equilibrium, and the ArgE concentration was constant throughout the duration of each experiment, thermodynamic parameters for the enzyme-catalyzed reaction were determined from an Arrhenius plot (Fig. 4a). The activation energy (E_a) for [Mn(II)_(ArgE)] is 50.3 kJ mol^{-1}. Determination of E_a in this manner allows subsequent resolution of other thermodynamic parameters by the following equations: $\Delta H^{\ddagger} = E_a - RT$, $\Delta S^{\ddagger} = (\Delta H^{\ddagger} - \Delta G^{\ddagger})/T$ and $\Delta G^{\ddagger} = -RT\ln(k_{cat} h/k_B T)$, where k_B, h, and R are the Bolzmann, Planck and gas constants, respectively. Therefore, ΔG

‡ = 58.1 kJ mol^{-1}, $\Delta H^{‡}$ = 47.8 kJ mol^{-1}, and $\Delta S^{‡}$ = −34.5 J mol^{-1} K^{-1} (Table 3). Similarly, a plot of ln(1/K_m) versus inverse temperature is linear over the same temperature range (Fig. 4b), so $\Delta H°$ was obtained as the negative slope times the gas constant. Since, $\Delta G° = RT\ln(1/K_m)$ and $\Delta S° = (\Delta H° - \Delta G°)/T$, the following thermodynamic parameters were determined for the Michaelis complex of NAO: $\Delta G°$ = 0.5 kJ mol^{-1}, $\Delta H°$ = −65.0 kJ mol^{-1}, and $\Delta S°$ = −220.0 J mol^{-1} K^{-1} (Table 3).

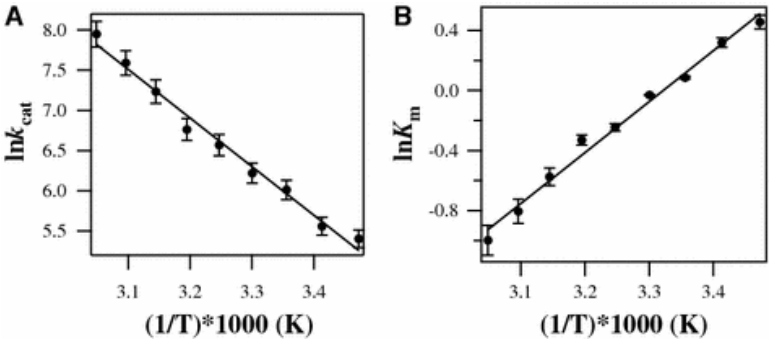

Fig. 4. Arrhenius plots of *N*-acetyl-l-ornithine (NAO) hydrolysis (**a**) and NAO binding (**b**) by [Mn(II)_(ArgE)]

Table 3. Thermodynamic parameters for the hydrolysis of l-leucine*p*-nitroanilide by Zn(II)-loaded AAP [47] compared with those for the hydrolysis of NAO by [Mn(II)_(ArgE)] and [Zn(II)_(ArgE)] [17] and [Co(II)_(ArgE)] [17]

	[Zn(II)Zn(II)(AAP)]	[Mn(II)_(ArgE)]	[Zn(II)_(ArgE)]	[Co(II)_(ArgE)]
E + S → ES				
$\Delta G°$ (kJ mol^{-1})	−6.1	0.5	ND	ND
$\Delta H°$ (kJ mol^{-1})	−42.6	−65.0	ND	ND
$\Delta S°$ (J mol^{-1} K^{-1})	−122.5	−219.9	ND	ND
ES → (ES··EP)‡				
$\Delta G^{‡}$ (kJ mol^{-1})	62.1	58.1	54.8	51.5
$\Delta H^{‡}$ (kJ mol^{-1})	34.0	47.8	23.2	31.8
$\Delta S^{‡}$ (J mol^{-1} K^{-1})	−94.2	−34.5	−106	−66.0
E_a (kJ mol^{-1})	36.5	50.3	25.6	34.3

AAP leucine aminopeptidase from *Aeromonas proteolytica* (*Vibrio proteolyticus*), *ND* not determined

Inhibition of Mn(II)-loaded ArgE by bestatin

The effect of bestatin binding on the [Mn(II)_(ArgE)]-catalyzed NAO hydrolysis was examined. Four data sets of kinetic assays repeated in triplicates using six concentrations of NAO (0.1–2.0 mM) were collected at different bestatin concentrations (0–500 μM). Plots of inverse velocity versus inverse substrate concentration were prepared and fit to the Michaelis–Menten equation for competitive inhibition as described by Cleland [40] (Fig. 5). The K_m value calculated for NAO hydrolysis in this experiment was 1.0 mM, in good agreement with K_m measurements of [Mn(II)_(ArgE)], while the K_i value for bestatin binding to ArgE was 67 μM. Since bestatin binding to other dinuclear metallohydrolases, like AAP has been described as a slow process [41], ArgE was preincubated with the appropriate concentrations of bestatin for up to 5 h prior to collection of kinetic data. No significant change to the inhibition constant was noted as a function of preincubation time with bestatin.

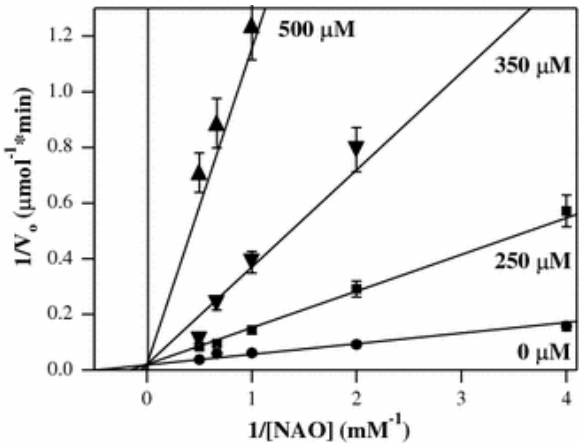

Fig. 5. Lineweaver–Burke plots, 1/*V* versus 1/[S] (where [S] is the substrate concentration), representing the inhibitory effect of 0, 250, 350, and 500 µM bestatin on NAO hydrolysis catalyzed by [Mn(II)_(ArgE)]

Spectroscopic characterization of Mn(II)-loaded ArgE

[Mn(II)_(ArgE)] exhibited an EPR spectrum typical of Mn(II) in an uconstrained environment (Fig. 6, spectrum A). The spectrum of [Mn(II)Mn(II)(ArgE)] exhibited more fine structure, including prominent features at approximately 1,500 G and at approximately 2,150 G (Fig. 6, spectrum B). The origins of these fine-structure features were further explored by examining spectra of (1) [Mn(II)Mn(II)(ArgE)] recorded at different temperatures (Fig. 7), (2) [Mn(II)Mn(II)(ArgE)] at pH 7.5 and pH 10.0 (Fig. 8), (3) heterodimetallic [Mn(II)Zn(II)(ArgE)] (Fig. 6, spectrum C), and (4) [Zn(II)Mn(II)(ArgE)] (Fig. 6, spectrum D). The predominant spectral features of [Mn(II)Mn(II)(ArgE)] at pH 7.5 exhibited indistinguishable, and essentially Curie–Weiss law, temperature dependencies from 6 to 30 K (Fig. 7). Closer examination of spectra recorded at 12 K showed no convincing evidence for Mn(II)–Mn(II) spin–spin coupling in [Mn(II)Mn(II)(ArgE)] at pH 7.5 (Fig. 8, spectra A and B), whereas [Mn(II)Mn(II)(ArgE)] at pH 10.0 (Fig. 8, spectra C and D) clearly showed the 45-G splitting expected for a dinuclear Mn(II)–Mn(II) center. The EPR spectra of [Mn(II)Zn(II)(ArgE)] (Fig. 6, spectrum C) and [Zn(II)Mn(II)(ArgE)] (Fig. 6, spectrum D) were distinct from that of [Mn(II)_(ArgE)] in that intense features due to fine structure were observable, though the spectra were different from each other and from that of [Mn(II)Mn(II)(ArgE)], particularly in terms of the intensities of the features at 4,000–5,000 G. The origin of the features in the spectra of the dimetallic forms of ArgE, other than the six-line $g \sim 2$ pattern, were investigated via computer simulation (Fig. 9). Subtraction of the spectrum of [Mn(II)_(ArgE)] from that of [Mn(II)Mn(II)(ArgE)] yielded the difference spectrum shown in Fig. 9, spectrum A and subtraction of the signal of [Zn(II)Mn(II)(ArgE)] from that of [Mn(II)Zn(II)(ArgE)] yielded the difference spectrum shown in Fig. 9, spectrum B. The computed spectrum (Fig. 9, spectrum C) assumes a single magnetically isolated Mn(II) ion with the spin-Hamiltonian parameters $g_{\text{isotropic}} = 2.0$, $A_{\text{isotropic}}^{I=5/2}(^{55}\text{Mn}) = 8.8 \times 10^{-3}$ cm^{-1}, $D = 0.093$ cm^{-1}, $\sigma D = 0.013$ cm^{-1}, and $E/D = 0.05$. The spectral density of the [Mn(II)Mn(II)(ArgE)] signal is asymmetric about the baseline in the 2,500–4,500-G region, suggesting rapid passage effects at the relatively high microwave field employed. Additional information is available from this phenomenon; subtraction of the superficially similar signal of [Mn(II)Zn(II)(ArgE)] from that of [Mn(II)Mn(II)(ArgE)] yielded an absorption signal (Fig. 6, spectrum E) in which each of the $M_{S=5/2}$ manifolds is evident. The EPR data, then, show that the Mn(II) ion(s) in the species [Mn(II)_(ArgE)], [Mn(II)Mn(II)(ArgE)], [Mn(II)Zn(II)(ArgE)], and [Zn(II)Mn(II)(ArgE)] are distinct. The Mn(II) ions in [Mn(II)Mn(II)(ArgE)] are magnetically isolated at physiologically significant pH but exhibit exchange coupling at higher, nonphysiological pH.

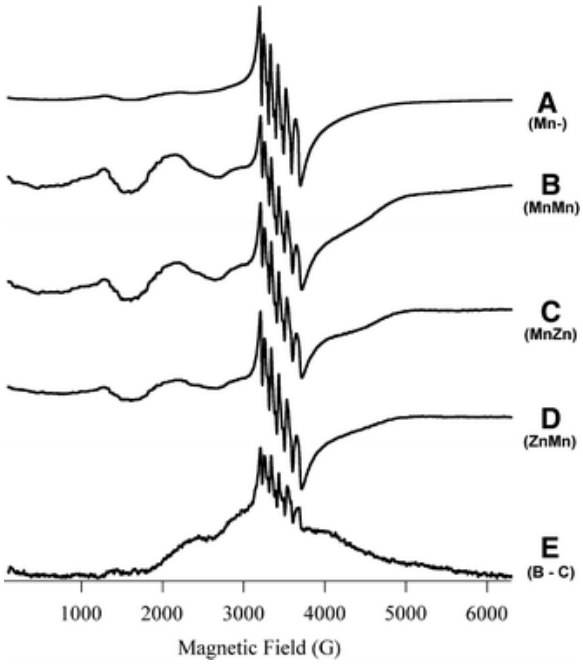

Fig. 6. Electron paramagnetic resonance (EPR) spectra of 1 mM samples of [Mn(II)_(ArgE)] (*A*), [Mn(II)Mn(II)(ArgE)] (*B*), [Mn(II)Zn(II)(ArgE)] (*C*), and [Zn(II)Mn(II)(ArgE)] (*D*), recorded at 9.63 GHz, 12 K, 20-mW microwave power in 50 mM HEPES buffer, pH 7.5. *E* A difference spectrum generated by subtracting a proportion of *C* from *B*

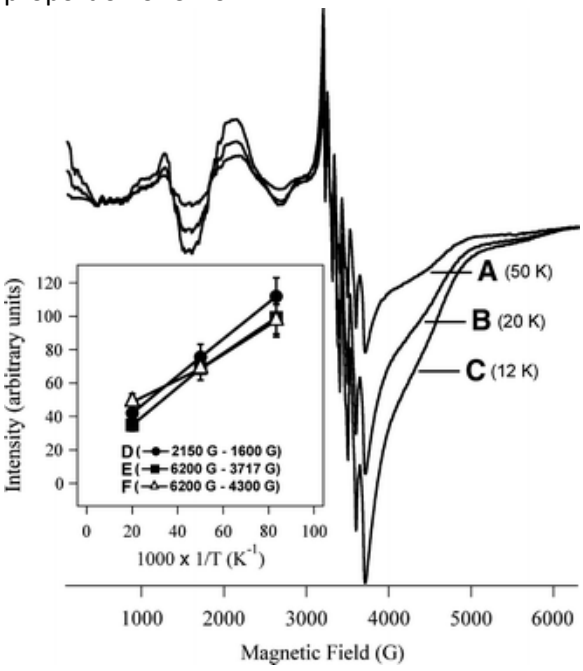

Fig. 7. EPR spectra of a 1 mM sample of [Mn(II)Mn(II)(ArgE)] recorded at 9.63 GHz, 20-mW microwave power in 50 mM HEPES buffer, pH 7.5, at 50 K (*A*), 20 K (*B*), and 12 K (*C*). The temperature dependencies of a low field fine structure feature (measured as $I_{D} = I_{2150\,G} - I_{1660\,G}$), of the high-field line of the central manifold (measured as $I_{E} = I_{6200\,G} - I_{3717\,G}$), and of the high field fine structure feature (measured as $I_{F} = I_{6200\,G} - I_{4300\,G}$) are plotted as *D*, *E*, and *F*, respectively

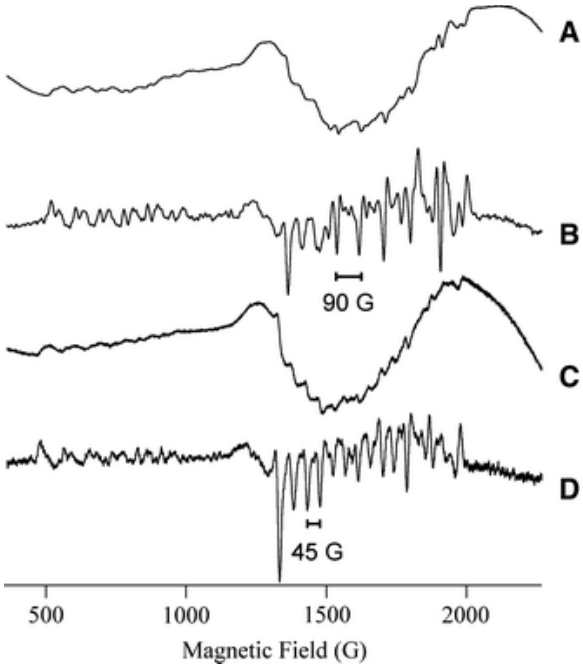

Fig. 8. Expanded EPR spectra of [Mn(II)Mn(II)(ArgE)] at pH 7.5 (*A*, *B*) and pH 10.0 (*C*, *D*). *A* and *C* show the as-recorded (9.63 GHz, 12 K, 20 mW) $\partial\chi''/\partial \boldsymbol{B}$ spectra, and *B* and *D* show the corresponding derivatives, $\partial^2\chi''/\partial \boldsymbol{B}^2$

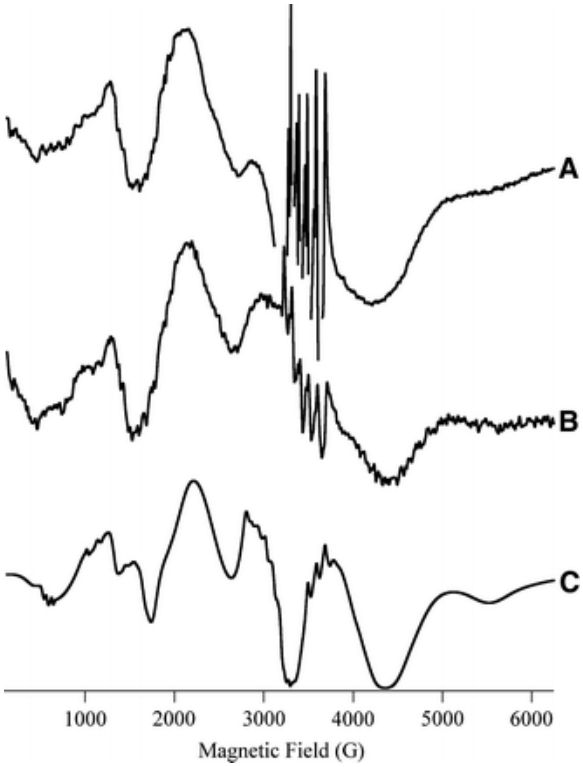

Fig. 9. A difference spectrum obtained by subtracting a proportion of spectrum A from spectrum B of Fig. 6. *B* Generated by subtraction of spectrum D from spectrum C of Fig. 6. *C* A theoretical spectrum generated using the parameters $g_{\text{isotropic}} = 2.0$, $A_{\text{isotropic}}{}^{I=5/2}$ (^{55}Mn) = 8.8×10^{-3} cm^{-1}, $D = 0.093$ cm^{-1}, $\sigma D = 0.013$ cm^{-1}, and $E/D = 0.05$

Upon the addition of bestatin, the spectra (Fig. 10) of [Mn(II)Mn(II)(ArgE)], [Mn(II)Zn(II)(ArgE)], and [Zn(II)Mn(II)(ArgE)] were all significantly perturbed. In each case, the intensity of the fine-structure feature at 1,200–1,450 G was diminished, and the feature evident in the spectra of untreated enzyme forms at around

2,100 G was shifted upfield by 200 G to 2,300 G. While the intensity of this feature was lowered upon the addition of bestatin in the cases of [Mn(II)Mn(II)(ArgE)] and [Mn(II)Zn(II)(ArgE)], the feature was enhanced for [Zn(II)Mn(II)(ArgE)].

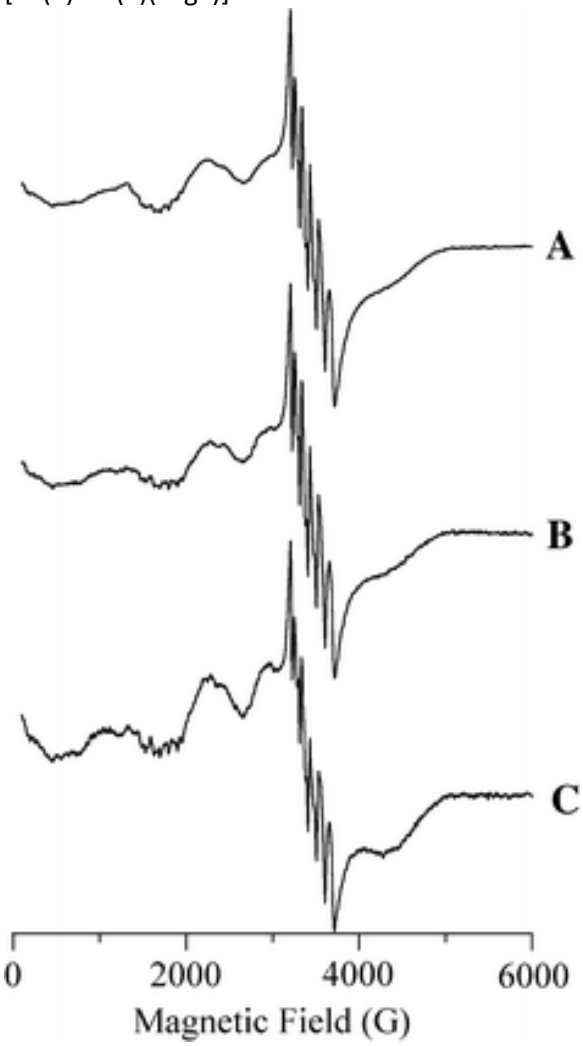

Fig. 10. EPR spectra of [Mn(II)Mn(II)(ArgE)] (*A*), [Mn(II)Zn(II)(ArgE)] (*B*), and [Zn(II)Mn(II)(ArgE)] (*C*) after incubation with bestatin in 50 mM HEPES buffer, pH 7.5. Spectra were recorded at 9.63 GHz, 12 K, 20-mW microwave power

Discussion

The arginine biosynthetic pathway offers several potential antibacterial targets that have yet to be explored [19]. One of the members of this pathway, ArgE, has been identified in several pathogenic bacteria such as *E. coli* O157:H7, *Salmonella typhimurium*, *Legionella pneumophila*, *Yersinia pseudotuberculosis*, *Bordetella pertussis*, *Vibrio cholerae*, *Staphylococcus aureus*, and *Mycobacterium tuberculosis* [11, 20, 21, 42]. Alignment of each of the gene sequences with the structurally characterized dinuclear Zn(II) metallohydrolases AAP and GCP_2 revealed significant sequence homology, especially in the amino acids functioning as metal ligands [21]. However, it should be noted that no catalytically important amino acid residues have been identified for any ArgE enzyme. Both AAP and CPG_2 possess a (μ-aquo)(μ-carboxylato)dizinc(II) core with one terminal carboxylate and histidine residue bound to each metal ion [22, 23]. The enzymatic activity of the ArgE from *E. coli* has recently been shown to be dependent on Zn(II) ions similar to AAP and CPG_2 [17, 21], but ArgE can also be activated by Mn(II) ions, unlike AAP and CPG_2 [17]. In an effort to gain insight into the structural and catalytic

properties of ArgE, we examined the Mn(II)-loaded forms via kinetic, thermodynamic, and spectroscopic methods.

ArgE shows nearly optimal kinetic activity in the presence of only 1 equiv of Mn(II). These data are similar to those reported for AAP, which exhibits approximately 90% of its total activity in the presence of one Zn(II) ion [43]. The k_{cat} and K_m values for ArgE loaded with 1 equiv of Mn(II) ([Mn(II)_(ArgE)]) were found to be 550 s^{-1} and 0.8 mM, respectively, providing a catalytic efficiency (k_{cat}/K_m) of 6.9×10^5 M^{-1} s^{-1}. The k_{cat}/K_m value for Mn(II)-loaded ArgE is only 2.8 and 4.6 times smaller than that observed for the Zn(II)-loaded enzyme and the Co(II)-loaded enzyme, respectively, suggesting that Mn(II) provides an ArgE enzyme that is nearly as capable as the Zn(II)-loaded form. The fact that ArgE can be activated by a number of first-row transition metal ions in the divalent oxidation state is typical for metallohydrolases in the M28 family [11]. However, Mn(II) does not, in general, activate these enzymes. For example, AAP cannot be activated by Mn(II) [44]; however, the *dapE*-encoded *N*-succinyl-l,l-diaminopimelic acid desuccinylase (DapE) from *Haemophilus influenzae* and blLAP, which is not a member of the M28 family, can both be activated by Mg(II) and Mn(II) [45]. ArgE shares no sequence homology with blLAP, but is 32% identical to AAP and retains all of the amino acid residues that function as metal ligands [21]. Such observations suggest ArgE may share structural homology with some enzymes and functional homology with others that are structurally distinct. Furthermore, the fact that ArgE is active with such a broad range of divalent metal ions suggests it might be critical to bacterial cell survival (i.e., if the cellular milieu is limiting in one metal, another can substitute).

Titration of apo-ArgE with Mn(II) confirmed that the enzyme is approximately 90% active after the addition of only 1 equiv of Mn(II). Fits of these titration data provided a K_d value for the first metal binding site of 180 nM. Since only one metal ion is bound to the enzyme active site, these K_d values correspond to the microscopic binding constants for the binding of a single metal ion to ArgE. This K_d value is significantly smaller than that observed for Zn(II) binding to ArgE (6 μM), but is similar to K_d values obtained for several other hydrolytic enzymes that contain mixed histidine-carboxylate active sites. For example, the K_d values for the first Zn(II) ion binding events in DapE and AAP are 140 and 1 nM, respectively [45]. Verification of the observed K_d value for the first metal binding site of ArgE was obtained from ITC. ITC measurements of Mn(II) binding to ArgE provided K_d values of 300 nM for the first metal binding site and 5.3 μM for the second. These data indicate that Mn(II) binds 9 times more tightly to the first metal binding site and 10 times more tightly to the second metal binding site than Zn(II) [17]. These data suggest that under physiological conditions in the absence of substrate, the second metal binding site is potentially only occupied when Mn(II) ions are present. For Mn(II), the first and second metal binding events are both endothermic, which differs from the case for both Zn(II) and Co(II), which exhibit exothermic first metal binding events and endothermic second metal binding events [17]. Interestingly, the Gibbs free energy does not significantly change upon substitution of Zn(II) by Mn(II) or Co(II) and is similar to that observed for AAP. Similarly, the entropic factor (ΔS) remains the same for the first metal binding event despite a large decrease in K_d for Mn(II) and Co(II) binding to ArgE. However, ΔS becomes negative for the second Mn(II) and Co(II) binding events but remains slightly positive for the second Zn(II) binding site. These data suggest a decrease in order around the second Mn(II) binding site.

Similar to AAP, ArgE binds 2 equiv of Mn(II), with ΔH_1 = 0.3 kJ mol^{-1} and ΔH_2 = 29.1 kJ mol^{-1} for AAP and ΔH_1 = 1.2 kJ mol^{-1} and ΔH_2 = 2.0 kJ mol^{-1} for ArgE. The binding affinity for Mn(II) at both sites on the basis of ITC measurements is similar for the two enzymes, K_{d1} = 3.4 μM and K_{d2} = 39 μM for AAP and K_{d1} = 0.3 μM and K_{d2} = 5.3 μM for ArgE. However, AAP is not catalytically competent when loaded with Mn(II) [44]. These data suggest that Mn(II) may bind to AAP and ArgE in a similar manner, but a Mn(II)-loaded AAP active site may not allow proper positioning of substrate for catalysis, while a Mn(II)-loaded ArgE site does. Thus, ArgE may also share functional homology with other dinuclear enzymes with which it shares little primary sequence homology, like the methionine aminopeptidase type II from *Homo sapiens*, which has been suggested to employ Mn(II) in vivo [46]. Therefore, efficacious pharmaceuticals targeting ArgE must incorporate functional groups that bind tightly and specifically to this active site in a variety of metal-loaded forms.

Since ArgE is relatively stable at 45 °C, activation parameters for the $ES^{‡}$ complex were obtained by examining the hydrolysis of NAO as a function of temperature. Construction of an Arrhenius plot from the temperature dependence of ArgE activity indicates that the rate-limiting step does not change as a function of temperature. The activation energy (E_a) for the $ES^{‡}$ complex of Mn(II)-loaded ArgE is 50.3 kJ mol^{-1}. The observed activation energy for Mn(II)-loaded ArgE is significantly larger than the E_a values reported for [Zn(II)_(ArgE)] (25.6 kJ mol^{-1}) and [Co(II)_(ArgE)] (34.3 kJ mol^{-1}) as well as the E_a values reported for AAP (36.5 kJ mol^{-1}) and DapE (31 kJ mol^{-1}) [17, 45, 47]. However, substrate binding to [Zn(II)Zn(II)(AAP)] [48] and [Mn(II)Mn(II)(ArgE)] appears to proceed by similar processes, since both enzymes are governed by a single rate constant, indicated by the linearity of a plot of $\ln(1/K_m)$ versus $1/T$ [49]. NAO binding to Mn(II)-loaded ArgE is distinguished by greater heat loss and a higher degree of order imposed by Michaelis complex formation. The possibility that the active sites of these metal-variant forms of ArgE are structurally different is supported by EPR data.

The EPR spectra of [Mn(II)_(ArgE)], [Mn(II)Mn(II)(ArgE)], [Mn(II)Zn(II)(ArgE)], and [Zn(II)Mn(II)(ArgE)] indicate distinct Mn(II) environments in each species (Fig. 6). Comparison of the signals observed for [Mn(II)_(ArgE)] and [Mn(II)Zn(II)(ArgE)] reveals a change in the environment of the Mn(II) ion upon binding a second metal ion. Subtraction of the signal of [Mn(II)_(ArgE)] from that of [Mn(II)Mn(II)(ArgE)] suggests an additional Mn(II) environment in [Mn(II)Mn(II)(ArgE)] that can be reasonably simulated as a magnetically isolated Mn(II) ion (Fig. 9). Similarly, subtraction of the signal of [Zn(II)Mn(II)(ArgE)] from that of [Mn(II)Zn(II)(ArgE)] isolated an analogous species. The asymmetry of the signal from [Mn(II)Mn(II)(ArgE)] indicated that one, or both, of the Mn(II) ions in that species exhibited unusually slow relaxation. This phenomenon was not observed in the other species and subtraction of the signal of [Mn(II)Zn(II)(ArgE)] from that of [Mn(II)Mn(II)(ArgE)] confirmed the presence of an absorption-like component in the spectrum of the latter. These relatively subtle differences between the spectra of each of the species illustrate a very important point; i.e., that both the existence and the nature of each metal ion in a dinuclear form of ArgE affects the electronic structure of the other. For example, the environment of Mn1 is affected by the binding of Zn ([Mn(II)_(ArgE)] versus [Mn(II)Zn(II)(ArgE)]). The effect of binding Mn2 upon the metal center of [Mn(II)Mn(II)(ArgE)] is to yield a slowly relaxing species that is not observed for Mn1 in [Mn(II)Zn(II)(ArgE)] or for Mn2 in [Zn(II)Mn(II)(ArgE)]; therefore, the nature of M1 and that of M2 influence each other's electronic structures. Furthermore, the lack of direct magnetic interaction between the Mn(II) ions in [Mn(II)Mn(II)(ArgE)] suggests that the mechanisms of these intermetal effects are likely structural in nature rather than magnetic. Thus, the active-site geometry in ArgE appears to be unusually dependent on the precise metal complement; the fine structure in *each* of the spectra from Mn(II)-loaded forms of ArgE was all assignable to magnetically isolated Mn(II) ions by simulation (Fig. 9) and temperature dependence (Fig. 7), and close examination of the fine structure (Fig. 8) provided no evidence for Mn(II)–Mn(II) spin coupling at pH 7.5.

The EPR spectrum of [Mn(II)Mn(II)(ArgE)] at pH 10.0 furnished clear evidence of a dinuclear Mn(II)-Mn(II) center, with a 45 G-split multiline pattern (Fig. 8). These data strongly suggest that the metal ions in the dinuclear forms of ArgE are in close proximity but are not bridged by a ligand capable of mediating exchange coupling at pH 7.5. The EPR signal for [Co(II)Co(II)(ArgE)] is not significantly altered between pH 7.5 and 10 [17], suggesting a hydroxide ion functions as the nucleophile for this enzyme form. On the other hand, the EPR signal for [Mn(II)Mn(II)(ArgE)] demonstrates spin coupling at pH 10, but not at pH 7.5. This suggests a water molecule acts as the nucleophile for this enzyme form at physiological pH, while a hydroxide is the nucleophile at pH 10. Such structural differences in Mn(II)-loaded ArgE might contribute to misalignment of the carbonyl carbon of substrate in the Michaelis complex. This would account for the higher activation energy of the transition state of Mn(II)-loaded ArgE compared with that of Co(II)-loaded and Zn(II)-loaded forms. The enthalpy of activation for Mn(II)-loaded ArgE at 25 °C is 47.8 kJ mol^{-1}, while the entropy of activation was found to be −34.5 J mol^{-1} K^{-1}. The positive enthalpy is indicative of a conformation change upon substrate binding, likely due to the energy of bond formation and breaking during nucleophilic attack on the scissile carbonyl carbon of the substrate. On the other hand, the negative entropy values suggest that some of the molecular motions are lost upon $ES^{‡}$ complex

formation, possibly owing to hydrogen-bond formation between catalytically important amino acids and the substrate. All of these factors contribute to the large positive free energy of activation.

Peptide analog inhibitors of microbiological origin have not been examined with an ArgE enzyme, but one of these, bestatin, has been shown to be a competitive, slow-binding inhibitor of both blLAP and AAP, with K_i^* values of 1.3 and 18 nM, respectively [35, 41, 52]. Bestatin is a naturally occurring dipeptide isolated from cultures of *S. olivoreticuli* and the metal binding region of bestatin has been designed into numerous dinuclear metallohydrolase inhibitors [52]. X-ray crystallographic data of bestatin-bound complexes of blLAP and AAP have been reported [53, 54]. The X-ray crystal structures of both [Zn(II)Zn(II)(blLAP)]–bestatin and [Zn(II)Zn(II)(AAP)]–bestatin revealed that the N-terminal amino group of bestatin coordinates to Zn2, while the alkoxide moiety bridges between the two Zn(II) ions. Interestingly, the backbone carbonyl oxygen of bestatin is not bound to the dinuclear metal center in blLAP but is, instead, hydrogen-bonded to the positively charged terminal amine of an active-site lysine residue. However, in AAP the backbone carbonyl oxygen of bestatin binds to Zn1. In order to determine if the metal binding region of bestatin can bind to the dinuclear active site of ArgE, the K_i for bestatin binding to Mn(II)-loaded ArgE was measured. Bestatin was found to be a simple competitive inhibitor of [Mn(II)Mn(II)(ArgE)], with a K_i of 67 μM. The presence or absence of a bridging water/hydroxide in the active site of Mn(II)-loaded ArgE was investigated by binding bestatin to [Mn(II)Mn(II)(ArgE)]. Only mild perturbation of the signal was observed in the EPR spectrum with bestatin, indicating binding to the active site, but not in a way that perturbs exchange coupling. These data indicate that bestatin binds to ArgE in a significantly different way from how it binds to AAP or blLAP [53, 54]. While bestatin does not bind ArgE tightly or specifically enough to be therapeutically practical, this dipeptide provides a backbone from which other molecules may be synthesized with increased and more specific binding affinity to the ArgE active site.

In conclusion, the kinetic and thermodynamic data presented herein provide evidence that two Mn(II) ions can bind to ArgE with K_d values that differ by a factor of approximately 18. Moreover, ArgE is nearly fully active upon the addition of one divalent Mn(II) ion. Therefore, ArgE behaves similarly to AAP where one metal ion is the catalytic metal ion, while the second is likely to play a structural role [47]. The spectroscopic data presented herein provide the first structural glimpse at the active site of a Mn(II)-loaded ArgE enzyme. EPR spectra of [Mn(II)Mn(II)(ArgE)] indicate clear evidence of spin–spin coupling between the two Mn(II) ions, but only at high pH values. In addition, bestatin was shown to be a competitive inhibitor of ArgE, but on the basis of EPR data, no bridging alkoxide moiety is present in the dimanganese(II) active site of ArgE. These data suggest that bestatin binds to ArgE enzymes in a way different from that observed by X-ray crystallography for AAP and blLAP [53, 54]. This finding is critical for the future design and synthesis of small molecule inhibitors, based on the metal binding components of bestatin that potentially target ArgE enzymes.

Acknowledgments

This work was supported by the National Science Foundation (CHE-0549221, R.C.H.) and the National Institutes of Health (AI056231, EB001980, B.B.).

References

1. Center for Disease Control and Prevention (1995) MMWR Morb Mortal Wkly Rep 44:1–13
2. Howe RA, Bowker KE, Walsh TR, Feest TG, MacGowan AP (1997) Lancet 351:601–602
3. Levy SB (1998) Sci Am 278:46–53
4. Chin J (1996) New Sci 152:32–35
5. Nemecek S (1997) Sci Am 276:38–39
6. Miller JB (2000) In: The pharmaceutical century. American Chemical Society, Washington, pp 52–71
7. Lesney MS, Frey R (2000) In: The pharmaceutical century. American Chemical Society, Washington, pp 110–129
8. Lesney MS, Frey R (2000) In: The pharmaceutical century. American Chemical Society, Washington, pp 92–109

9. Lesney MS, Tweedy BD (2000) In: The pharmaceutical century. American Chemical Society, Washington, pp 72–91
10. Loefler I-J-P (1996) Lancet 348:21–28
11. Holz RC, Bzymek K, Swierczek SI (2003) Curr Opin Chem Biol 7:197–206
12. Bradshaw R, Yi E (2002) Essays Biol Med 38:65–78
13. Daiyasua H, Osakaa K, Ishinob Y, Toha H (2001) FEBS Lett 503:1–6
14. Lipscomb WN, Sträter N (1996) Chem Rev 96:2375–2433
15. Wilcox DE (1996) Chem Rev 96:2435–2458
16. Dismukes GC (1996) Chem Rev 96:2909–2926
17. McGregor W, Swierczek SI, Bennett B, Holz RC (2005) J Am Chem Soc 127:14100–14107
18. Cunin R, Glansdorff N, Pierard A, Stalon V (1986) Microbiol Rev 50:314–352
19. Girodeau J-M, Agouridas C, Masson M, Pineau R, LeGoffic F (1986) J Med Chem 29:1023–1030
20. Meinnel T, Schmitt E, Mechulam Y, Blanquet S (1992) J Bacteriol 174:2323–2331
21. Javid-Majd F, Blanchard JS (2000) Biochemistry 39:1285–1293
22. Chevrier B, Schalk C, D'Orchymont H, Rondeau J-M, Moras D, Tarnus C (1994) Structure 2:283–291
23. Rowsell S, Pauptit RA, Tucker AD, Melton RG, Blow DM, Brick P (1997) Structure 5:337–347
24. Baker JO, Prescott JM (1983) Biochemistry 22:5322–5331
25. Baker JO, Prescott JM (1985) Biochem Biophys Res Commun 130:1154–1160
26. Baker JO, Wilkes SH, Bayliss ME, Prescott JM (1983) Biochemistry 22:2098–2103
27. Prescott JM, Wilkes SH (1976) Methods Enzymol 45:530–543
28. Lejczak B, Kafarski P, Zygmunt J (1989) Biochemistry 28:3549–3555
29. Bennett B, Holz RC (1998) J Am Chem Soc 120:12139–12140
30. Sträter N, Lipscomb WN (1995) Biochemisty 34:9200–9210
31. Wilkes SH, Prescott JM (1983) J Biol Chem 258:13517–13521
32. Wilkes SH, Prescott JM (1987) J Biol Chem 262:8621–8625
33. Chan WWC, Dennis P, Demmer W, Brand K (1982) J Biol Chem 257:7955–7957
34. Umezawa HT, Aoyagi T, Suda H, Hamada M, Takeuchi T (1976) J Antibiot (Tokyo) 29:97–99
35. Wilkes SH, Prescott JM (1985) J Biol Chem 260:13154–13162
36. Carpenter FH, Vahl JM (1973) J Biol Chem 248:294–304
37. Gill SC, von Hippel PH (1989) Anal Biochem 182:319–326
38. Bennett B, Holz RC (1997) J Am Chem Soc 119:1923–1933
39. Bennett B, Holz RC (1997) Biochemistry 36:9837–9846
40. Cleland WW (1979) Methods Enzymol 63:103–138
41. Taylor A, Peltier CZ, Torre FJ, Hakamian N (1993) Biochemistry 32:784–790
42. Gibbs JB (2000) Science 287:1969–1973
43. Prescott JM, Wagner FW, Holmquist B, Vallee BL (1983) Biochem Biophys Res Commun 114:646–652
44. Bayliss ME, Prescott JM (1986) Biochemistry 25:8113–8117
45. Bienvenue DL, Gilner DM, Davis RS, Bennett B, Holz RC (2003) Biochemistry 42:10756–10763
46. Wang J, Sheppard GS, Lou P, Kawai M, Park C, Egan DA, Schneider A, Bouska J, Lesniewski R, Henkin J (2003) Biochemistry 42:5035–5042
47. Chen G, Edwards T, D'souza VM, Holz RC (1997) Biochemistry 36:4278–4286
48. Bzymek KP, Holz RC (2004) J Biol Chem 279:31018–31025
49. Laidler KJ, Peterman BF (1979) Methods Enzymol 63:234–257
50. D'souza VM, Brown RS, Bennett B, Holz RC (2005) J Biol Inorg Chem 10:41–50
51. Copik AJ, Nocek B, Swierczek SI, Ruebush S, SeBok J, D'souza VM, Peters J, Bennett B, Holz RC (2004) Biochemistry 43:121–129
52. Huntington KM, Bienvenue D, Wei Y, Bennett B, Holz RC, Pei D (1999) Biochemistry 38:15587–15596Stamper C, Bienvenue D, Moulin A, Bennett B, Ringe D, Petsko G, Holz RC (2004) Biochemistry 43:9620–9628
53. Burley SK, David PR, Lipscomb WN (1991) Proc Natl Acad Sci USA 88:6916–6920